



Simulation of the strain distribution under a two-dimensional sand pile

Pradip Roul ^{a,b,*}, Alexander Schinner ^c, Klaus Kassner ^b

^a Institute of Applied Mathematics, Potsdam University, Potsdam, D-14469, Germany

^b Institute of Theoretical Physics, Otto-von-Guericke University Magdeburg, Postfach 4120, D-39106 Magdeburg, Germany

^c T-Systems, Dachauer Straße 665, D-80995 München, Germany

ARTICLE INFO

Article history:

Received 25 November 2010

Received in revised form 25 May 2011

Accepted 28 August 2011

Available online 3 September 2011

Keywords:

Numerical simulation

Sand pile

Stress

Strain

Granular matter

Discrete-element method

ABSTRACT

We study the averaged macroscopic strain tensor for a sand pile consisting of soft convex polygonal particles numerically, using the discrete-element method (DEM). First, we construct two types of “sand piles” by two different pouring protocols. Afterwards, we deform the sand piles, relaxing them under a 10% reduction of gravity. Four different types of methods, three best-fit strains and a derivative strain, are adopted for determining the strain distribution under a sand pile. The results of four different versions of strains obtained from DEM simulation are compared with each other. Moreover, we compare the vertical normal strain tensor between two types of sand piles qualitatively and show how the construction history of the piles affects their strain distribution.

© 2011 Elsevier B.V. All rights reserved.

1. Introduction

Most of the time we handle granular materials in our everyday life. Examples of such granular materials include sand, rice, small seed, powders, pills and many others. Among these, sand plays an important role in various industries such as mining, agriculture and civil engineering. Clearly, it is also important for geological processes. Sand piles (stockpiles) stand out due to their high technological relevance: the storage of granular materials in the form of a sand pile occurs in many industrial situations. Moreover, sand piles are of fundamental importance to practical applications, such as silos and dams.

The stress distribution in granular media is important in many situations including silo design, foundation building as well as for the constructions of roads and dams. On the other hand, the study of deformation of granular materials under external loading is also of practical importance for many industries. Therefore, the understanding of the basic physical principles behind the distributions of stress and strain in stationary granular materials is very important.

The pressure or stress distribution under a sand pile exhibits puzzling properties. In some cases, it shows a local minimum (dip) below the tip of the pile, in others, it does not [1–4]. What is observed depends strongly on the construction history of the sand pile. Moreover, the size and shape distributions of particles influence the stress distributions of sand piles [5–7], both in two-dimensional [5] and three-

dimensional [7] setups. Determining stress fields inside sand piles has, for various reasons, been one of the more interesting tasks of researchers on granular materials in the physics community, experimentally [1,5–10], theoretically [4,11–16] and numerically [2,3,17–20]. To a certain extent, even more interesting than to study the stress tensor is to determine the strain tensor inside the piles, in order to establish a correlation between the stress and strain tensors, and to evaluate effective material properties of the piles, which will help improve our understanding of transport, construction and processing problems appearing in particulate materials. It is worth mentioning that strain fields have not been measured so far in experiments on sand piles and analytical models assume that for sand piles strain fields are not available. Therefore, constitutive relations proposed for the equations describing sand piles [4,11–16] have been obtained without employing the strain tensor.

We focus on investigating numerically the averaged strain under a sand pile, constructed either from a point source or a line source, by employing four different types of approaches, three best-fit methods including Cambou's strain [21], Cundall's strain [22], and Liao's strain [23], and a simple differentiation method. Then the results are checked for consistency, i.e., we examine whether the four different versions of strains are in good agreement with each other.

This paper is organized as follows. In Section 2, we describe details of the simulation setup. In Section 3, we determine the strain tensor adopting four different approaches. We then present simulation results on the strain distributions of two-dimensional sand piles in Section 4. Section 5 summarizes our results. An appendix explains the force calculation part of the algorithm, which is essential for its closeness to reality.

* Corresponding author at: Institute of Mathematics, Potsdam University, Potsdam, D-14469, Germany. Tel.: +49 17620961836; fax: +49 3319771578.

E-mail address: drprkroul@yahoo.com (P. Roul).

2. Simulation method

We use the discrete-element method (DEM) originally developed by Cundall and Strack [22] for the simulation of particulate materials to generate sand piles consisting of soft particles. Numerical simulations were performed on two-dimensional systems, in which a sand pile was constructed from convex polygons with varying shapes, sizes and edge numbers. Polygons were used as it is believed that particle shape does play a certain role in determining the properties of static assemblies of granular matter. Therefore, whereas much of the dynamics of flowing granular matter may be captured by simulations with circular or spherical particles, such a favorable situation cannot be expected for a granulate that is mechanically at rest. Real sand grains vary in shape and might be approximated reasonably by polyhedral particles in a simulation. However, the algorithmic complexity of a simulation of many polyhedra is formidable; to our knowledge, no good approach to force calculation for these three-dimensional objects has been proposed so far, and collision detection, while algorithmically less challenging, is pretty difficult, too. For two-dimensional systems, we have to deal with polygons only, which renders the task feasible. Of course, this takes some of the realism out of our simulations, but the basic phenomena to be discussed have been observed experimentally both in two- and three-dimensional assemblies so that we may expect to be able to learn something from simulations in two dimensions (2D) as well.

The particles were poured either from a point source (*wedge sequence*) or a line source (*layered sequence*). Static and dynamic friction forces are accounted for in our force law, which enables us to simulate the relaxation of sand piles to their final static state.

The basic structure of DEM consists of a simple loop that is composed of three steps: collision detection, force calculation and time integration. In order to determine the position and orientation of each particle, we solve Newton's and Euler's equations of motion (1), using an explicit algorithm, a fifth-order Gear predictor–corrector method [24], usually with a fixed time step:

$$\begin{aligned} m_i \ddot{\mathbf{r}}_i &= \mathbf{F}_i + \sum_{j=1}^n \mathbf{F}_{ij} \\ I_i \ddot{\phi}_i &= T_i + \sum_{j=1}^n T_{ij}. \end{aligned} \quad (1)$$

Here, m_i and $\ddot{\mathbf{r}}_i$ denote the mass and linear acceleration of particle i . \mathbf{F}_i is the external force acting on particle i ; in our problem, gravity is the only external force acting on the particles. \mathbf{F}_{ij} is the force produced by the particle touching particle i in contact j . T_{ij} is the torque about the center of mass generated by this force, and T_i , accordingly, is the torque by the external force. With gravity as the only external force, we have $T_i = 0$ for all i , since a homogeneous gravitational field does not produce a torque about the center of mass (more or less by definition). I_i and $\ddot{\phi}_i$ are the moment of inertia and angular acceleration of particle i about its center of mass, respectively. The angles ϕ_i are measured with respect to some arbitrary but fixed direction. The first of Eq. (1) is vectorial, the second scalar (because we work in 2D).

We use soft particles in simulations, meaning that particles can interpenetrate partially. From a theoretical point of view, the most interesting case would rather be that of completely rigid particles, first, because this is a good approximation to the sand piles we have in mind, second, because in such a pile strains would be a truly macroscopic property, arising solely from particle displacements due to rearrangements and not from deformation of the particles themselves. To set up such a simulation, contact dynamics [25–27] would be the method of choice. However, contact dynamics is algorithmically very demanding and, what is worse, does not scale linearly with particle number, thus limiting rather severely the size of systems that can be simulated. In order to avoid the problems arising from

static indeterminacy of rigid particles, it would then be advantageous to assign a small amount of deformability to the particles. But to solve the elastic equations for each collision between pairs of nonrigid particles would be inefficient. Hence, we do not allow shape changes. Instead, we calculate forces between particles from their overlap during a collision. The larger this overlap, the stronger the repulsive force. While an in-depth description of the force calculation algorithm may be found in our previous work [28,29], we collect some of the details in an appendix for the convenience of the reader and to make this article more self-contained.

An additional advantage of our approach is that it may be easily adapted to both static and dynamic simulations without major changes.

We constructed two types of symmetric sand piles from about 6500 particles by adopting two different pouring protocols – the 14 piles and 11 piles were built from point source and line source procedures, respectively. The detailed construction procedures for the two types of sand piles are given in [30]. The corner number of the particles varies from 6 to 8 in each simulation. We used a static friction coefficient of $\mu = 0.54$ for the particles, and the same value in the dynamic friction coefficient (reasons are given in the appendix).

For the precise definition of the simulation parameters the values of which we give now, we refer the reader to the appendix. The density ρ and Young's modulus Y of the particles were chosen equal to 5000 kg/m^3 and 10^7 N/m , respectively. We did not implement cohesion in these simulations as we are interested in the behavior of cohesionless granular aggregates. The time step for constructing the sand piles was $2 \times 10^{-6} \text{ s}$, and damping coefficient (explained in the appendix) was $\gamma = 0.75$. Particles were inscribed into ellipses, the principal axes of which (aligned horizontally and vertically) were drawn independently from uniform distributions. Here, the average was taken equal to 6.8 mm for both axes and both types of sand piles. The degree of polydispersity was 30%, meaning that the interval, from which the axes were drawn extended from 0.7 times the average to 1.3 times the average.

The average angle of repose, a result rather than an input quantity, was obtained by taking the average over the left and right base angles of the sand piles and found to be about 28° and 27° for point source and line source sand piles, respectively.

Once we have the forces and their points of contact, we can determine the stress tensor of a single particle. The stress tensor of a single particle can be expressed as follows:

$$\sigma_{ij} = \frac{1}{V^p} \sum_{c=1}^n x_i^c f_j^c, \quad (2)$$

where x_i^c is i -th component of the branch vector jointing from the center of mass of the particle to the contact point c , and f_j^c is the j -th component of the total force in that contact point. The summation in Eq. (2) is over all contact points of the particle p . V^p is the volume of the particle (it is an area in two-dimensions).

This microscopic stress tensor is not a meaningful quantity to describe the macroscopic sand pile, so we have to average over many particles in a representative volume element (RVE) for a continuum description. The size of the RVE is determined from the requirement to obtain converged results. We determined this size and found consistent results using boxes containing 100–200 particles.

3. Determining strains

We deform the sand piles by slowly reducing gravity from the ambient gravity level of the pile at $g = 9.81 \text{ m/s}^2$. Our original idea was to define strain fields with respect to a hypothetical reference state of zero gravity of a pile essentially equivalent to the one at ambient gravity, except for slightly changed positions of the particle centers of mass. The reference state would then be reached

from the actual one by reducing gravity slowly. In principle, it is not necessary to go down to zero gravity, as long as the strains increase linearly with the gravity level. Instead, one may then extrapolate to zero from the knowledge of the positions of the particle centers of mass at two arbitrary different gravity levels. Of course, linearity has to be checked by looking at different gravity levels of the piles.

This procedure does not work as expected, since a reduction of gravity leads to a linear reduction only of normal stresses corresponding to the direction of gravity, i.e. σ_{yy} , but not horizontal stresses, i.e., σ_{xx} . The reason behind this is that σ_{xx} is essentially determined by horizontal static friction. Since the frictional contacts need not be fully mobilized, there is no strict proportionality between lateral forces and gravity, when we change gravity slowly. Let us define μ_{eff} to be the true proportionality coefficient between the friction force F_{\parallel} at a contact and the normal force F_{\perp} on it, $\mu_{eff} = |F_{\parallel}/F_{\perp}|$, then we have $0 \leq \mu_{eff} \leq \mu$, the left-hand equality corresponding to contacts that are not mobilized at all, while the right-hand one describes fully mobilized contacts, i.e. contacts that will become sliding as soon as the tangential force F_{\parallel} gets a little larger. The fact that μ_{eff} may change during a modification of the gravity level destroys the desired linearity property. In order to verify this phenomenon, we first created three different types of sand piles separately with different gravity levels of $g=9.81 \text{ m/s}^2$, $g=5 \text{ m/s}^2$ and $g=20 \text{ m/s}^2$, where the particles were poured from a point source, which means three sand piles were constructed using the same simulation parameters except for the value of gravity acceleration. We then measured numerically the vertical normal stress σ_{yy} and the horizontal normal stress σ_{xx} inside the resulting sand piles. They are illustrated in Fig. 1. On the left-hand side of the figure, panels (A), (B) and (C), respectively, show the vertical normal stresses for the sand piles at $g=9.81 \text{ m/s}^2$, $g=5 \text{ m/s}^2$ and $g=20 \text{ m/s}^2$, whereas on the right-hand side, panels (D), (E) and (F) show the corresponding horizontal normal stresses. It can be seen that in this case the vertical and horizontal normal stresses are proportional to the gravity level as

expected. On the other hand, when we measure the stresses for a sand pile created at $g=9.81 \text{ m/s}^2$ after slowly changing gravity levels to $g=5 \text{ m/s}^2$ and $g=20 \text{ m/s}^2$, respectively, the vertical normal stress σ_{yy} remains proportional to gravity, but the horizontal normal stress σ_{xx} does not as the simulation results shown in Fig. 2 demonstrate. Note that the maximum of σ_{xx} changes by a factor of 2 only, that of σ_{yy} by a factor of 4, corresponding to the factor in g . Moreover, we arrived at the same conclusions for the shear stress σ_{xy} as it is proportional to the gravity level when we created separately three different types of sand piles with different gravity levels of $g=9.81 \text{ m/s}^2$, $g=5 \text{ m/s}^2$ and $g=20 \text{ m/s}^2$ as represented in Fig. 3, whereas it is not when we change gravity levels from $g=9.81 \text{ m/s}^2$ to $g=5 \text{ m/s}^2$ or from $g=9.81 \text{ m/s}^2$ to $g=20 \text{ m/s}^2$ (see Fig. 4).

For sand piles created at different gravity levels, all three stress components (σ_{yy} , σ_{xx} , σ_{xy}) scale with gravity, indicating that the distribution of effective friction coefficients and hence the degree of mobilization of contacts is the same. However, if we reduce gravity for a pile created at ambient gravity, contacts not fully mobilized need not reduce their friction force and may become mobilized instead. So the distribution of μ_{eff} will shift towards higher values, σ_{xx} will be reduced by a smaller amount than proportionality would dictate. An increase of the gravity level will lead to a reduction in the degree of mobilization, shifting effective friction coefficients to smaller values.

Nevertheless, it is of course still possible to determine incremental strains, which are defined as the strain changes between the actual state and a state at a different gravity level. Using incremental stresses and strains, one can determine macroscopic elastic constants inside the piles.

We employ three different versions of best-fit strains proposed by Cambou et al. [21], Cundall et al. [22], Liao et al. [23], and a simple differentiation method for determining the macroscopic strain tensor inside the sand piles. The results of these four different versions of strains obtained from DEM simulation have to be compared with each other.

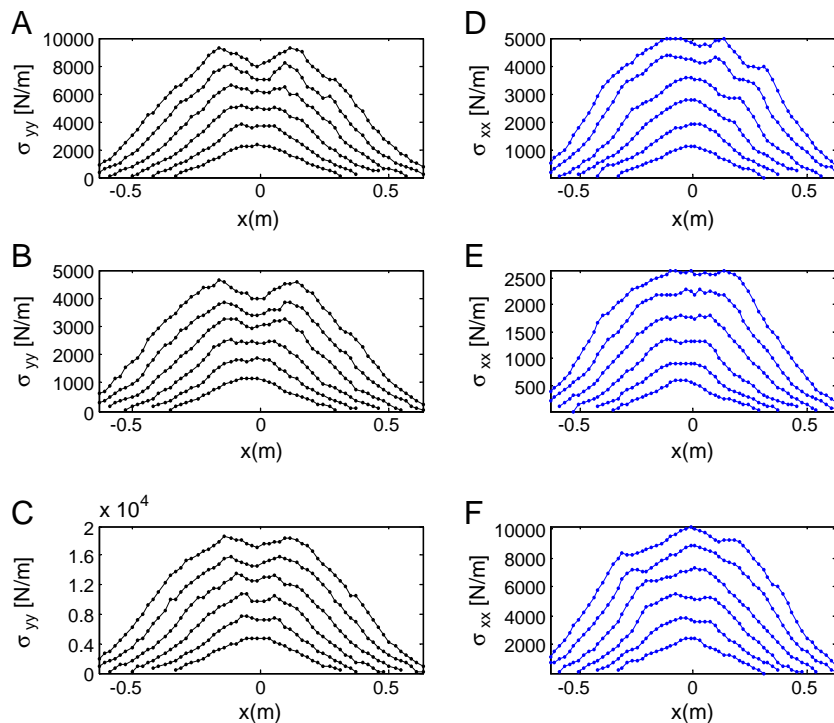


Fig. 1. Vertical (σ_{yy}) and horizontal (σ_{xx}) components of stress tensor at three different gravity levels of sand piles that were constructed separately by pouring particles from a point source with $g=9.81$, $g=5$, and $g=20$. In panel (A) we give σ_{yy} at $g=9.81$, in (B) σ_{yy} at $g=5$, in (C) σ_{yy} at $g=20$, in (D) σ_{xx} at $g=9.81$, in (E) σ_{xx} at $g=5$, and in (F) σ_{xx} at $g=20$.

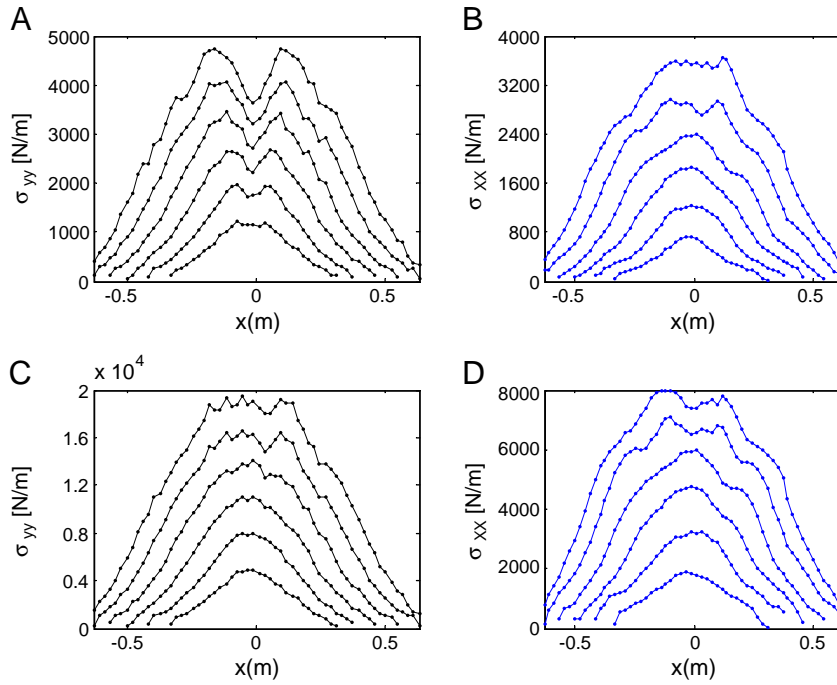


Fig. 2. Vertical (σ_{yy}) and horizontal (σ_{xx}) components of stress tensor at two gravity levels, first one obtained by reducing gravity from the actual state (ambient gravity level) to a state at $g=5$, second one obtained by increasing gravity to $g=20$. (a) σ_{yy} at $g=5$, (b) σ_{yy} at $g=20$, (c) σ_{xx} at $g=5$, and (d) σ_{xx} at $g=20$. These are to be compared with panels (A) and (D) of Fig. 2.

The best-fit strains are based on the idea that a translation gradient is obtained which gives the smallest deviation from the characteristic displacements of an assembly of grains. The term characteristic displacement means the translation of the particle center or the relative translation of a contact point, the latter involving rotation of the particles around their centers. We determine the translation of the individual particle center, rotation of the particles, and relative translation of two particles at the contact by considering two different

gravity levels of sand piles. One is the actual state of the sand pile at a gravity level of $g=9.81 \text{ m/s}^2$ and the second one is obtained by reducing gravity slowly by about 10% from that ambient gravity level. In the following subsections, we discuss three different kinds of least-square fit strains along with a derivative strain known as:

- The best-fit strains of Cambou et al.,
- Cundall's best-fit strain,
- The best-fit strains of Liao et al.
- Derivative method.

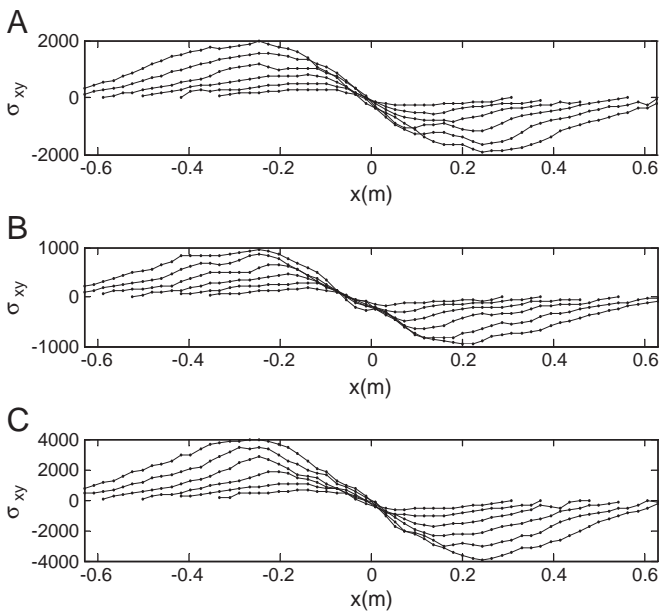


Fig. 3. Shear stresses (σ_{xy}) at three different gravity levels of sand piles that were constructed separately by pouring particles from a point source with $g=9.81$, $g=5$, and $g=20$. In panel (A) we give σ_{xy} at $g=9.81$, in (B) σ_{xy} at $g=5$, in (C) σ_{xy} at $g=20$.

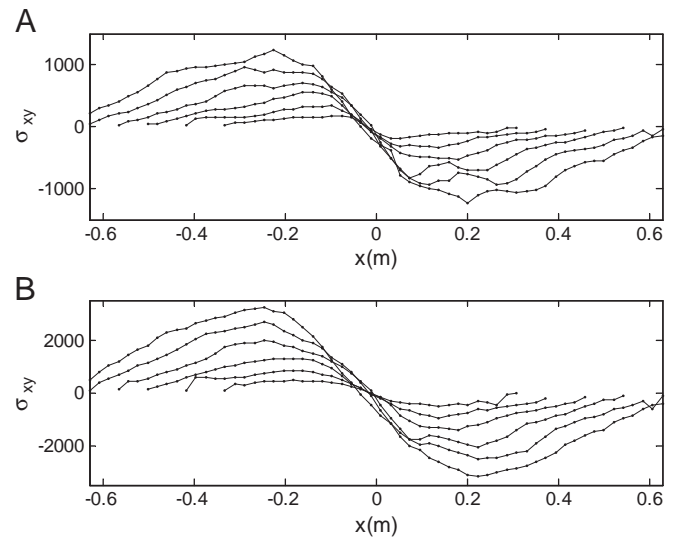


Fig. 4. Shear stress at two gravity levels, first one obtained by reducing gravity from the actual state to a state at $g=5$, second one obtained by increasing gravity to $g=20$. (a) σ_{xy} at $g=5$, and (b) σ_{xy} at $g=20$.

Clearly, our two-dimensional simulation cannot faithfully represent the three-dimensional modes of deformation of a sand pile, because in 3D, while it is possible to impose either a stress or a strain field that depends on two Cartesian coordinates only, hence is two-dimensional, there is always a coupling of the conjugate field to the third dimension. For example, if the stress distribution is truly two-dimensional, a situation depicted as plane stress, then the strain has a non-vanishing component along the third direction [for isotropic linear elasticity, $u_{zz} = -\frac{\nu}{1-\nu}(u_{xx} + u_{yy})$, ν is Poisson's ratio]; on the other hand, if the strain distribution is purely two-dimensional, a case named plane strain, then the stress has a non-vanishing third normal component [for isotropic linear elasticity, $\sigma_{zz} = \nu(\sigma_{xx} + \sigma_{yy})$]. So there is no satisfactory mapping from the two-dimensional case to the three-dimensional one. Nevertheless, the basic phenomena, such as the pressure minimum in sand piles are known to occur in 2D as well as in 3D, so qualitative conclusions may still be drawn from two-dimensional simulations. Moreover, experiments with two-dimensional sand piles have been done [5]. The particles in [5] were not really much smaller in one spatial direction than in the others, a situation that would have corresponded to plane stress, but since the cases of plane stress and plane strain can be mapped onto each other by a simple transformation of the Poisson ratio (while keeping the shear modulus constant), our simulations (which correspond to the assumption of plane strain) would have relevance to experiments of this kind.

3.1. Cambou's best-fit strain

This method was proposed by Cambou et al. [21] who consider the relative translation instead of the contact deformations and exclude particle rotations from the analysis. Displacements are characterized in terms of the translations of the particle centers.

Let us assume that two grains p and q have a contact c and du_j^p denotes the translation of the center of particle p along axis $[i = x(\hat{=} 1)$ or $i = y(\hat{=} 2)]$. The relative translation of the pairs of grains p and q forming contact c is

$$d\Delta u_j^c = du_j^q - du_j^p. \quad (3)$$

Let r_i^{pc} and r_i^{qc} be the contact vectors joining from the corresponding particle centers to the contact point c . According to Cambou et al. the branch vector assigned to a contact is defined as $l_i^c = r_i^{pc} - r_i^{qc}$, as illustrated in Fig. 5, i.e., it is simply the difference of the center-of-mass vectors of the two particles sharing the contact c (usually, these center-of-mass vectors are called branch vectors, but Cambou et al. use a different convention).

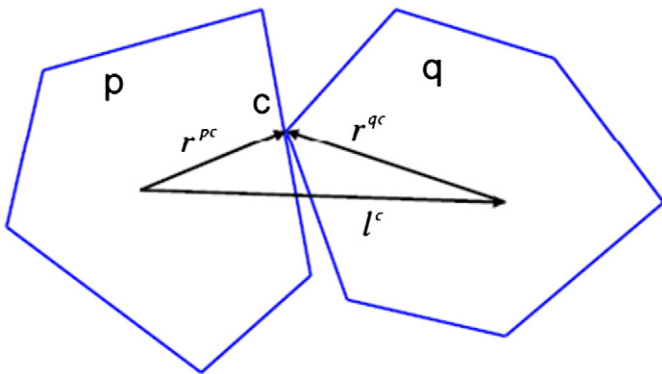


Fig. 5. Schematic diagram of Cambou's branch vector l^c assigned to the contact c of two particles. Note that according to our preceding nomenclature r^{pc} and r^{qc} are the branch vectors.

If every particle of an assembly of grains moved according to a uniform translation gradient tensor ε_{ji} , then the relative translation of the two particles would be

$$d\Delta u_i^c = \varepsilon_{ji} l_j^c. \quad (4)$$

However, usually microscopic displacements do not have uniform gradients, and in a general case, we would have

$$d\Delta u_i^c \neq \varepsilon_{ji} l_j^c. \quad (5)$$

Then, we determine the tensor ε_{ji} for which the square sum of the deviations from Eq. (5) is smallest i.e., we minimize the following quantity

$$Z = \sum_{c=1}^n (d\Delta u_j^c - \varepsilon_{ji} l_j^c)^2 \quad (6)$$

with respect to ε_{kl} , i.e., we set $\frac{\partial Z}{\partial \varepsilon_{kl}} = 0$ for every pair k, l .

Eq. (6) gives four equations in 2D which can be written in matrix form as follows

$$\begin{pmatrix} \sum_{c=1}^n l_1^c l_1^c & \sum_{c=1}^n l_2^c l_1^c \\ \sum_{c=1}^n l_1^c l_2^c & \sum_{c=1}^n l_2^c l_2^c \end{pmatrix} \begin{pmatrix} \varepsilon_{1i} \\ \varepsilon_{2i} \end{pmatrix} = \begin{pmatrix} \sum_{c=1}^n d\Delta u_i^c l_1^c \\ \sum_{c=1}^n d\Delta u_i^c l_2^c \end{pmatrix} \quad (i \text{ is } 1 \text{ or } 2). \quad (7)$$

Let Z_{ij} denote the inverse of the coefficient matrix. In order to determine the ε_{11} and ε_{21} we substitute $i = 1$, whereas $i = 2$ is substituted for the calculation of ε_{12} and ε_{22} . The solution of Eq. (7) can be written in the general form

$$\varepsilon_{ij} = Z_{ik} \sum_c d\Delta u_j^c l_k^c, \quad i, j = 1, 2. \quad (8)$$

The tensor ε_{ij} in Eq. (8) is the best-fit translation gradient of Cambou et al. [21]. The components of the strain tensor in 2D are as follows

$$\varepsilon_{xx}(x, y) = \sum_c d\Delta u_x^c (z_{11} l_x^c + z_{12} l_y^c)$$

$$\varepsilon_{yy}(x, y) = \sum_c d\Delta u_y^c (z_{21} l_x^c + z_{22} l_y^c)$$

$$\varepsilon_{xy}(x, y) = \sum_c d\Delta u_y^c (z_{11} l_x^c + z_{12} l_y^c)$$

$$\varepsilon_{yx}(x, y) = \sum_c d\Delta u_x^c (z_{21} l_x^c + z_{22} l_y^c).$$

We note that the strain tensor u_{ij} is obtained from the above equations by symmetrization, i.e. $u_{ij} = \frac{1}{2}(\varepsilon_{ij} + \varepsilon_{ji})$.

3.2. Cundall's best-fit strain

This best-fit strain was proposed by Cundall et al. [22], the strain tensor is calculated by considering the translations of the particle centers, while particle rotations are not taken into consideration.

Let x_i^p be the i -th component of the initial position of the center of mass of particle p in the actual state of a sand pile in a two-dimensional system. The translation of the center of particle p is denoted as du_i^p and N is the total number of particles within the averaging volume element. A particle is considered inside the volume element, if its center of mass lies inside it.

The average of the i -th component of the position vectors of particle centers inside the averaging element is

$$X_i' = \frac{1}{N} \sum_{p=1}^N X_i^p, \quad (9)$$

and the average of the particle translations inside the averaging element is

$$dU_i' = \frac{1}{N} \sum_{p=1}^N du_i^p. \quad (10)$$

The deviations of the individual particle positions can be calculated with

$$X_i^p = x_i^p - X_i'. \quad (11)$$

And the deviations of the relative translations of the individual particles with respect to the average translation are determined from:

$$dU_i^p = (du_i^p - dU_i'). \quad (12)$$

If each particle inside the averaging volume element moved exactly according to a uniform translation gradient tensor ε_{ij} , the relative translation of individual particle would be

$$dU_i^p = \varepsilon_{ji} X_j^p. \quad (13)$$

However, usually this is not the case, hence, we would not find any ε_{ij} satisfying Eq. (13), in short

$$dU_i^p - \varepsilon_{ji} X_j^p \neq 0. \quad (14)$$

Instead, we determine the tensor ε_{ij} for which the square sum of the deviations in Eq. (14) is smallest i.e., we minimize the following expression

$$Z = \sum_p (dU_i^p - \varepsilon_{ji} X_j^p)^2 \quad (15)$$

with respect to ε_{ji} , i.e. we set $\frac{\partial Z}{\partial \varepsilon_{kl}} = 0$ for every k, l .

Eq. (15) provides four equations in 2D which can be expressed in a matrix form as follows

$$\begin{bmatrix} \sum_p X_1^p X_1^p & \sum_p X_1^p X_2^p \\ \sum_p X_2^p X_1^p & \sum_p X_2^p X_2^p \end{bmatrix} \begin{bmatrix} \varepsilon_{1i} \\ \varepsilon_{2i} \end{bmatrix} = \begin{bmatrix} \sum_p dU_i^p X_1^p \\ \sum_p dU_i^p X_2^p \end{bmatrix} \quad (i \text{ is } 1 \text{ or } 2). \quad (16)$$

Let w_{ij} denote the inverse of the coefficient matrix. In order to determine the components of strain tensors ε_{11} and ε_{21} we substitute $i = 1$, whereas $i = 2$ is substituted for the calculation of ε_{12} and ε_{22} .

The solution of Eq. (16) can be written in the general form

$$\varepsilon_{ij} = w_{ik} \sum_p dU_j^p X_k^p \quad i, j = 1, 2. \quad (17)$$

The tensor ε_{ij} in Eq. (17) is the best-fit translation gradient of Cundall et al. The components of the strain tensor in two dimensions are as follows

$$\varepsilon_{xx}(x, y) = \sum_p dU_x^p (w_{11} X_x^p + w_{12} X_y^p)$$

$$\varepsilon_{yy}(x, y) = \sum_p dU_y^p (w_{21} X_x^p + w_{22} X_y^p)$$

$$\varepsilon_{xy}(x, y) = \sum_p dU_y^p (w_{11} X_x^p + w_{12} X_y^p)$$

$$\varepsilon_{yx}(x, y) = \sum_p dU_x^p (w_{21} X_x^p + w_{22} X_y^p).$$

3.3. The best-fit strain of Liao et al.

This approach has been proposed by Liao et al. [23] and the definition is based on similar ideas to those of Cundall's best-fit strain and Cambou's best-fit strain, but instead of considering center-of-mass translation of the particle, Liao et al. consider displacements of the contact points in the calculation of contact deformation which means that they have to take into account particle rotation besides particle translation.

Let us consider two particles p_1 and p_2 touching each other at the contact point c . The vectors $r_i^{p_1c}$ and $r_i^{p_2c}$ are the branch vectors joining from the particle centers to the contact point. Now, we can define the translation of p_1c and p_2c , given by

$$du_i^{p_1c} = du_i^{p_1} + \beta_{ijk} r_j^{p_1c} d\theta_k^{p_1}, \quad (18)$$

$$du_i^{p_2c} = du_i^{p_2} + \beta_{ijk} r_j^{p_2c} d\theta_k^{p_2}, \quad (19)$$

where $du_i^{p_1}$ denotes the translation of the center of mass of the particle p_1 , while $d\theta_k^{p_1}$ signifies rotation of the particle p_1 about its center. β_{ijk} is the permutation symbol.

The contact deformation de_i^c at the contact c would be

$$de_i^c = du_i^{p_2c} - du_i^{p_1c}. \quad (20)$$

In general, every particle does not move exactly according to a uniform translation gradient tensor, hence we have

$$de_i^c - \varepsilon_{ji} l_j^c \neq 0, \quad (21)$$

where l_j^c is the j -th component of the vector joining the centers of mass of the two particles p_1 and p_2 sharing contact c .

Similar to the case of the definition of Cundall and Cambou strains, we determine the tensor ε_{ij} for which the sum of the deviations square in Eq. (21) is the smallest.

Therefore, we minimize the following quantity with respect to ε_{ji} ,

$$Z = \sum_c (de_i^c - \varepsilon_{ji} l_j^c)^2 \quad (22)$$

i.e. we set $\frac{\partial Z}{\partial \varepsilon_{kl}} = 0$ for every k, l .

Again we obtain four equations in 2D which can be written in a matrix form as follows

$$\begin{bmatrix} \sum_c l_1^c l_1^c & \sum_c l_2^c l_1^c \\ \sum_c l_1^c l_2^c & \sum_c l_2^c l_2^c \end{bmatrix} \begin{bmatrix} \varepsilon_{1i} \\ \varepsilon_{2i} \end{bmatrix} = \begin{bmatrix} \sum_c de_i^c l_1^c \\ \sum_c de_i^c l_2^c \end{bmatrix} \quad i = 1, 2. \quad (23)$$

The solution of Eq. (23) can be written in the general form

$$\varepsilon_{ij} = z_{ik} \sum_c de_j^c l_k^c \quad i, j = 1, 2. \quad (24)$$

where z_{ij} denotes the inverse of the coefficient matrix on the left-hand side of Eq. (23). The components of the strain tensor in two dimensions are as follows

$$\varepsilon_{xx}(x, y) = \sum_c de_x^c (z_{11} l_x^c + z_{12} l_y^c)$$

$$\varepsilon_{yy}(x, y) = \sum_c de_y^c (z_{21} l_x^c + z_{22} l_y^c)$$

$$\varepsilon_{xy}(x, y) = \sum_c de_y^c (z_{11} l_x^c + z_{12} l_y^c)$$

$$\varepsilon_{yx}(x, y) = \sum_c de_x^c (z_{21} l_x^c + z_{22} l_y^c).$$

3.4. Derivative method

We derive a formula for the strain tensor by using the derivative of the particle displacement, which means that the particle rotations are not used in the calculation of the strain tensor. The displacement vector of a single particle reads

$$u_i = x_i - x_i', \quad (25)$$

where x_i is the initial position of the center of mass of particle i and x_i' is the final position of the center of mass of the particle after applying an overload to the sample. Then, we take an average over individual displacements of the particles inside the volume element to determine a continuous displacement field as a function of the point position (x, y) .

$$u_i(x, y) = \frac{1}{n} \sum_{i=1}^n u_i \quad (26)$$

The sum is over the particles in an averaging volume element centered at (x, y) . This procedure allows us to determine the components of the strain tensor at the point considered. The simplest approximation for the three components of the strain tensor in two dimensions (which are linear combinations of derivatives of the displacements) is as follows

$$\begin{aligned} u_{yy}(x, y) &= \frac{u_y(x, y + h_y) - u_y(x, y)}{h_y} \\ u_{xx}(x, y) &= \frac{u_x(x + h_x, y) - u_x(x, y)}{h_x} \\ u_{xy}(x, y) &= \frac{0.5(u_x(x, y + h_y) - u_x(x, y))}{h_y} + \frac{0.5(u_y(x + h_x, y) - u_y(x, y))}{h_x} \end{aligned} \quad (27)$$

where h_x and h_y are the distances between the centers of the neighboring averaging volume element along the x and y directions and the center of the current one, respectively.

4. Simulation results

Here, we are interested in determining the strains using four different versions of strain tensors (the three best-fit strains and the derivative strain) using the Eqs. (8), (17), (24), and (27) by numerical investigation, and to compare the results for the vertical normal strain tensor quantitatively. The results of the average (negative) vertical normal strain at the bottom layer of the sand pile constructed from a line source are illustrated in Fig. 6. All the strain tensors were measured via imposing a 10% reduction of gravity from the ambient gravity level.

For the case of a line source, we have averaged results over seven sand piles in order to reduce fluctuations. We observe from Fig. 6 that the best-fit strains of Cambou et al. and Cundall et al. are close to each other with a deviation of few percent, while the best fit strain of Liao et al. significantly differs from the Cambou strain and Cundall strain, the deviation going up to 30–40%. The reason for this large deviation may be the inclusion of particle rotations in the calculation of the Liao strain, instead of consideration of only the translation of the particle center. Possibly, the Liao strain might be useful in theories employing micro-polar continua and involving couple stresses in addition to force stresses. Then micro-rotation effects may partially compensate

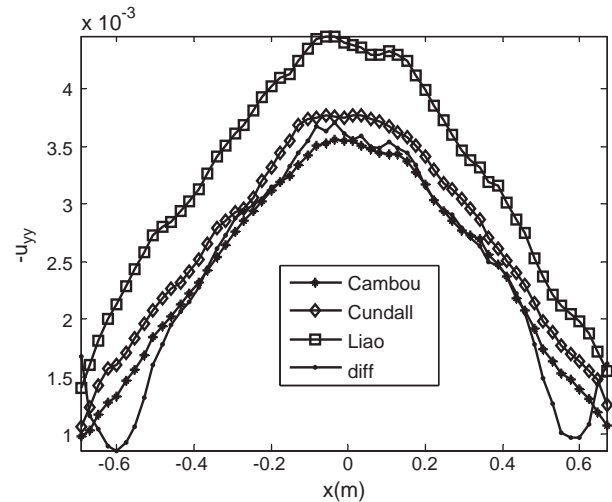


Fig. 6. Vertical normal strain tensor at the bottom layer of the sand pile constructed from a line source obtained using four different approaches.

for the excess strains of Liao et al. As long as we assume a symmetric stress tensor, the other strain definitions appear to be more useful.

On the other hand, the vertical normal (negative) strain obtained using the differentiation method shows a behavior different from that of the other strains especially in the vicinity of the surface of the sand pile, but is similar to them near the center of the sand pile. It is in good quantitative agreement with the best-fit strains of Cambou et al. and Cundall et al. Clearly, numerical differentiation should be avoided whenever possible and the deviations near the extremities of the sand pile are artifacts of the procedure.

Furthermore, we compared the results of the four types of strains quantitatively for sand piles constructed from a point source. Fig. 7 gives the simulation results of average negative vertical normal strains at the bottom layer of the point source sand pile. For the point source case, we averaged the strains over seven sand piles each. Again, quantitative comparison indicates strong deviations for the Liao strain and exhibits the deficiencies of the differentiation method.

Moreover, the vertical normal strain shows a dip (Fig. 7) near the center of the piles that are poured from a point source. On the other hand, the vertical normal strain increases towards the center and towards the bottom layer of sand piles poured from a line source, i.e., a

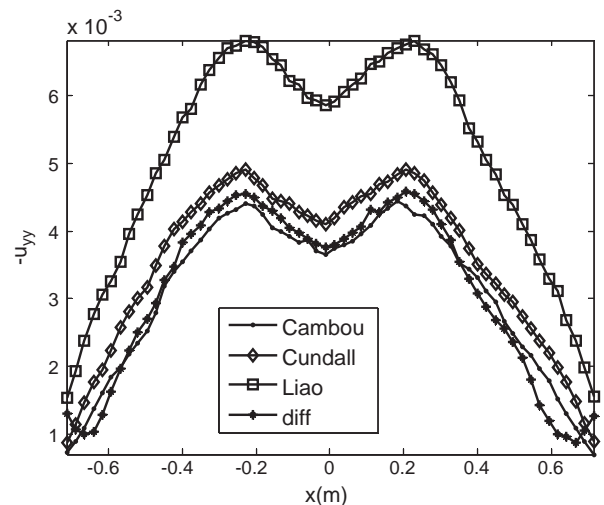


Fig. 7. Vertical normal strain tensor at the bottom layer of the sand pile constructed from a point source obtained using four different approaches.

strain dip does not occur in sand piles constructed from a line source, see Fig. 6.

5. Conclusion

To obtain a measure for strain, the sand pile was allowed to relax under reduction of gravity. We define strain with respect to a hypothetical reference state of a pile at zero gravity. This reference state may be approximated using a static pile obtained in a simulation, by slowly changing gravity and following the particle trajectories during the ensuing load change and then extrapolating to zero gravity, as has been discussed in Section 3. This procedure gives a decent approximation for the vertical strain u_{yy} , but is only qualitative for u_{xx} and u_{xy} . Incremental strains can be measured precisely, because they do not require the definition of a particular reference state. Then it is easy to compute the macroscopic strain tensor by averaging over an RVE.

The averaged strain tensor was evaluated for two types of sand piles that were built using two different pouring procedures. We find that the vertical normal strain u_{yy} shows a dip below the apex of the pile constructed from a point source. A similar vertical normal strain minimum was not obtained in piles poured from a line source, which demonstrates that the construction history affects the strain distribution under a sand pile.

To optimize our strain calculations, the strain tensor was evaluated by adopting three different types of best-fit methods including Cambou et al. [21], Cundall et al. [22], and Liao et al. [23], and also by simple differentiation of the displacement particle centers. Simulations showed that the strains obtained by Cambou et al., Cundall et al. and the differentiation method give similar results, whereas the strain obtained using Liao et al. exhibits different behavior. The closeness of the results from three out of the four methods in most of the pile suggests consistency of these strain calculations.

Simulation results of stress and strain tensor may serve for a determination of nonlinear stress–strain relationships for sand piles. Moreover, the constitutive relations proposed for sand pile models so far are in terms of the stress tensor only and it would be interesting to develop better constitutive relations using the stress and strain tensors.

Acknowledgement

This work was supported by a grant of the German Science Foundation (DFG) and the Land Sachsen-Anhalt within the graduate school GK 828. The authors acknowledge numerous useful discussions with Prof. Stefan Luding.

Appendix: calculation of contact forces

A completely realistic approach to the calculation of a contact force should start from the elastic properties of the two colliding particles and their deformation on impact, then take into account plastic contributions when strains become large and finally include a good friction model. However, such an approach is not practical given the huge number of collisions we wish to treat in a decent amount of time and the numerical cost of the solution of partial differential equations.

Instead, we allow particles to overlap without shape change, but introduce a repulsive force that increases strongly with increasing overlap of a pair of particles thus mimicking the effects of elastic (and possibly plastic) deformation. Fig. 8 visualizes the geometrical elements relevant to the calculation. Due to the convexity of overlapping particles, their boundaries will intersect in exactly two points c_1 and c_2 , as soon as there is a finite overlap area. The straight line joining these points is the contact line, used to define a normal direction \mathbf{n}_\perp and a tangential direction \mathbf{n}_\parallel as well as the point where contact

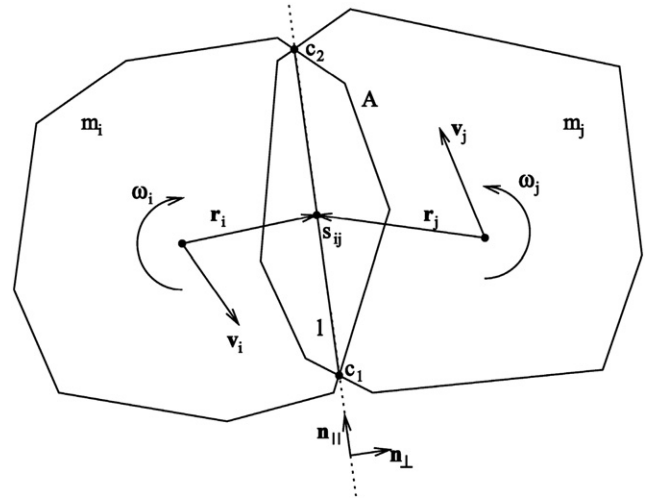


Fig. 8. Illustration of geometrical and dynamical quantities used in the calculation of two colliding particles. This is a close-up and much more detailed version of Fig. 5. The size of the overlap area (not shown in Fig. 5) is strongly exaggerated.

forces act, for which its midpoint s_{ij} is taken. Since we assume equal density for all particles, the particle masses m_i and m_j are directly proportional to the corresponding particle areas. The contact point s_{ij} is also needed in the definition of the branch vectors \mathbf{r}_i and \mathbf{r}_j pointing to it from the centers of mass of the particles. The overlap area A is calculated using the surveyor's formula for the inner polygon containing the corners c_1 and c_2 . Dynamical quantities entering the force calculation are the particle velocities \mathbf{v}_i and \mathbf{v}_j and the angular frequencies of particle rotation, ω_i and ω_j .

First we define a few quantities needed in the calculation. The characteristic or contact length is given by $l = \frac{r_i r_j}{r_i + r_j}$, where $r_i = |\mathbf{r}_i|$, $r_j = |\mathbf{r}_j|$ (so it is not the length of the contact line). This is half the harmonic mean of the branch vector lengths corresponding to the common contact of the two particles. If one of the particles is much smaller than the other, l becomes equal to its branch vector length. This choice of a characteristic length accounts for the fact that the same elastic displacement is much more easily imposed on a large body than on a small one, or to put it differently that short springs are stiffer than long ones. Next, we introduce a reduced mass via $m_\perp = \frac{m_i m_j}{m_i + m_j}$, and a “tangential” mass $m_\parallel = \frac{1}{\frac{1}{m_i} + \frac{1}{m_j} + \frac{r_i^2}{I_i} + \frac{r_j^2}{I_j}}$, where I_i and I_j are the mo-

ments of inertia of the particles with respect to their centers of mass [see also Eq. (1)], calculable from their polygonal shape assuming homogeneous mass density. The tangential velocity of one particle referred to the other is $\mathbf{v}_i = (\mathbf{v}_1 - \mathbf{v}_2 + \mathbf{r}_1 \times \boldsymbol{\omega}_1 - \mathbf{r}_2 \times \boldsymbol{\omega}_2) \cdot \mathbf{n}_\parallel$. We define a penetration depth using the overlap area A and the characteristic length l : $d_{eff} = A/l$. This depth is essentially proportional to the overlap area, as the characteristic length changes very little during a collision. With these definitions, the contact force consists of three contributions.

- (i) An elastic repulsive force normal to the contact length:

$$F_\perp = Y d_{eff} = Y \frac{A}{l}.$$

Here, the particle Young's modulus Y is used for the first time.

- (ii) A dissipative normal force to account for the fact that collisions are almost always inelastic: This force is constructed in two steps. First, we set

$$D_\perp^* = \gamma \sqrt{Y m_\perp} d_{eff} = \gamma \sqrt{Y m_\perp} \frac{\Delta A}{l \Delta t},$$

where the second formula follows from the assumption that l is constant during the collision. γ is a damping coefficient. Now it

can happen that $|D_{\perp}^*|$ becomes larger than $|F_{\perp}|$, which is not a problem when the two particles approach each other. But if this occurs while they move away from each other, then the resulting force will be attractive which is unphysical. Hence the dissipative part of the normal force is set according to the following rule

$$D_{\perp} = \begin{cases} D_{\perp}^* & \text{on approach} \\ \max(D_{\perp}^*, -F_{\perp}) & \text{on separation} \end{cases}$$

- (iii) A tangential friction force F_{\parallel} following the work of Cundall and Strack [22]: To be able to model Coulomb friction, we use the following procedure. Whenever two particles touch, an imaginary spring is attached to the contact point. This spring is elongated during the continuing sliding motion of the particles alongside each other. A restoring force of the spring will then start to build up. Of course, this force cannot become arbitrarily large, so the spring will not be elongated any further, when the maximum force allowed by the static friction coefficient has been reached. Instead the spring is pulled along the contact line, sliding at fixed extension. Clearly, the tangential force does not *have* to reach the maximum value μF_{\perp} , because it acts to reduce v_{\parallel} , and once the relative tangential motion of the two particles stops, the spring is also not elongated any further. The spring is removed when a contact opens up. At initiation of a new contact, we set $F_{\parallel}(0) = 0$ and afterwards, the tangential force evolves according to

$$F_{\parallel}^*(t + \Delta t) = \min\left(F_{\parallel}^*(t) + \frac{2}{7} \gamma v_{\parallel} \Delta t, \mu F_{\perp}(t)\right),$$

where μ is the static friction coefficient, and the factor $\frac{2}{7}$ is adapted to Hertzian stress for spherical particles. For a sliding contact, μ should be replaced by the dynamic friction coefficient, which in our simulations is taken equal to the static coefficient. This allows us to get around the necessity of deciding whether a contact is sliding or not (which is nontrivial, as the exact value zero of the velocity is numerically infrequent). In order to avoid or reduce spurious oscillations of the tangential velocity, a viscous damping term is introduced for the tangential force similar to the procedure used in the calculation of the normal force. Setting

$$D_{\parallel} = v_{\parallel} \sqrt{\frac{2}{7} Y m_{\parallel}},$$

we compute the total tangential force as

$$F_{\parallel}^*(t + \Delta t) = \pm \min\left(\left|F_{\parallel}^*(t) + \frac{2}{7} \gamma v_{\parallel} \Delta t + D_{\parallel}\right|, |\mu F_{\perp}(t)|\right),$$

with the sign chosen appropriately, so the force will always be opposite to the relative tangential motion of the two particles. In total, three parameters enter the force model; these are the particle Young's modulus Y , the phenomenological viscosity γ , and the friction coefficient μ . The particle Young's modulus is a phenomenological coefficient, too, since it may differ by a (small) factor from the true bulk Young's modulus, given that the normal elastic displacement is assumed proportional to, but not necessarily equal to, A/l .

Advantages of the described modeling procedure are that a particle sliding with a small velocity on a substrate (for which another big particle may serve) will not commence

continuous oscillations and that a particle is able to come to rest on an inclined plane, both features that our force model should have in the interest of realism.

References

- [1] L. Vanel, D. Howell, D. Clark, R.P. Behringer, E. Clement, Memories in sand: experimental tests of construction history on stress distributions under sand piles, *Physical Review E* 60 (1999) R5040.
- [2] H.-G. Matuttis, Simulation of the pressure distribution under a two-dimensional heap of polygonal particles, *Granular Matter* 1 (1998) 83–91.
- [3] H.-G. Matuttis, S. Luding, H.J. Herrmann, Discrete element simulations of dense packings and heaps made of spherical and non-spherical particles, *Powder Technology* 109 (2000) 208–292.
- [4] J. Teichman, Wu Wei, FE-Calculations of stress distribution under prismatic and conical sand piles within hypoplasticity, *Granular Matter* 10 (2008) 399–405.
- [5] I. Zuriguel, T. Mullin, J.M. Rotter, Effect of particle shape on the stress dip under a sand pile, *Physical Review Letters* 98 (2007) 028001.
- [6] I. Zuriguel, T. Mullin, The role of particle shape on the stress distribution in a sand pile, *Proceedings of the Royal Society A* 464 (2008) 99–116.
- [7] R. Brockbank, J.M. Huntely, R. Ball, Contact force distribution beneath a three-dimensional granular pile, *Journal de Physique II* 7 (1997) 1521–1532 (France).
- [8] T. Jotaki, R. Moriyama, On the bottom pressure distribution of the bulk materials piled with the angle of repose, *Journal of the Society of Powder Technology, Japan* 16 (1979) 184–191 (in Japanese).
- [9] J. Smid, J. Novosad, Pressure distribution under heaped bulk solids, *Particle Technology: Proceedings of the Powtech Conference*. Rugby, Institution of Chemical Engineers, D3V, 1981, pp. 1–12.
- [10] Y.C. Zhao, B.H. Xu, R.P. Zou, A.B. Yu, P. Zulli, Stress distribution in a sand pile formed on a deflected base, *Advanced Powder Technology* 14 (2003) 401–410.
- [11] A.K. Didwania, F. Cantelaube, J.D. Goddard, Static multiplicity of stress states in granular heaps, *Proceedings of the Royal Society of London A* 456 (2000) 2569–2588.
- [12] J.P. Wittmer, M.E. Cates, P. Claudin, Stress propagation and Arching in Static Sand piles, *Journal de Physique I* 7 (1997) 39–80 (France).
- [13] F. Cantelaube, J.D. Goddard, Elastoplastic arching in 2D granular heaps, in: R.P. Behringer, J.T. Jenkins (Eds.), *Powders and Grains*, Balkema, Rotterdam, 1997, pp. 231–234.
- [14] J.-P. Bouchaud, M.E. Cates, P. Claudin, Stress distribution in Granular media and nonlinear wave equation, *Journal de Physique I* 5 (1995) 639–656 (France).
- [15] J.P. Wittmer, M.E. Cates, P. Claudin, J.-P. Bouchaud, An explanation for the stress minimum in sand piles, *Nature* 382 (1996) 336–338.
- [16] P. Claudin, J.-P. Bouchaud, M.E. Cates, J. Wittmer, Models of stress fluctuations in granular media, *Physical Review E* 57 (1998) 4441.
- [17] S. Luding, Stress distribution in static two-dimensional granular model media in the absence of friction, *Physical Review E* 55 (1997) 4720–4729.
- [18] K. Liffman, D.Y.C. Chan, B.D. Hughes, On the stress depressions under a sand pile, *Powder Technology* 78 (1994) 263–271.
- [19] Y.J. Li, Y. Xu, C. Thornton, A comparison of discrete element simulations and experiments for 'sand piles' composed of spherical particles, *Powder Technology* 160 (2005) 219–228.
- [20] P. Roul, A. Schinner, Simulation study on micro and macro mechanical behaviour of sand piles, *Powder Technology* 204 (2010) 113–123.
- [21] B. Cambou, M. Chaze, F. Dedecker, Change of scale in granular materials, *European Journal of Mechanics – A/Solids* 19 (2000) 999–1014.
- [22] P.A. Cundall, O.D.L. Strack, A discrete numerical model for granular assemblies, *Geotechnique* 29 (1979) 47–65.
- [23] C.L. Liao, T.P. Chang, D.H. Young, C.S. Chang, Stress–strain relationship for granular materials based on the hypothesis of best fit, *International Journal of Solids and Structures* 34 (1997) 4087–4100.
- [24] C.W. Gear, *Numerical Initial Value Problems in Ordinary Differential Equations*, Prentice-Hall, 1971.
- [25] M. Jean, J.J. Moreau, Unilaterality and friction in the dynamics of rigid body collections, *Proceedings of Contact Mechanics International Symposium*, Presses Polytechniques et Universitaires Romandes, Lausanne, 1992, pp. 31–48.
- [26] J.J. Moreau, Some numerical methods in granular dynamics, *Powders & Grains*, 93, Balkema, Rotterdam, 1993, p. 227.
- [27] M. Jean, The non-smooth contact dynamics method, *Computer Methods in Applied Mechanics and Engineering* 177 (1999) 235–257.
- [28] A. Schinner, Ein Simulationssystem für granulare Aufschüttungen aus Teilchen variabler Form. PhD thesis, Univ., Magdeburg, 2001.
- [29] P. Roul, A. Schinner, K. Kassner, Mechanical properties of non-cohesive polygonal particle aggregates, *Granular Matter* (2010), doi:10.1007/s10035-010-0228-1 (online first).
- [30] P. Roul, A. Schinner, K. Kassner, Discrete-Element computation of averaged tensorial fields in sand piles consisting of polygonal particles. *Geotech. Geol. Eng.*, DOI: 10.1007/s10706-011-9406-0.